A new device for the generation of microbubbles

José M. Gordillo[a)]
Grupo de Mecánica de Fluidos, Escuela Superior de Ingenieros, Universidad de Sevilla,
Camino de los Descubrimientos s/n, 41092 Sevilla, Spain

Zhengdong Cheng
Department of Physics and Division of Engineering and Applied Sciences, Harvard University, Cambridge,
Massachusetts 02138

Alfonso M. Ganan-Calvo
Escuela Superior de Ingenieros, Universidad de Sevilla, Ingenieria Energetica y Mecanica de Fluidos,
Camino de los Descubrimientos s/n, 41092 Sevilla, Spain

M. Márquez
Los Alamos National Laboratory, Chemistry Division, Los Alamos, New Mexico 87545
and Computational Chemistry Group, Physical and Chemical Properties Division,
National Institute of Standards and Technology, Gaithersburg, Maryland 20899

D. A. Weitz[b)]
Department of Physics and Division of Engineering and Applied Sciences, Harvard University, Cambridge,
Massachusetts 02138

In this paper we present a new method for the production of bubble-liquid suspensions (from now on BLS) composed of micron-sized bubbles and with gas to liquid volume ratios larger than unity. We show that the BLS gas fraction $\lambda = Q_g/Q_l$, being Q_g and Q_l the flow rates of gas and liquid, respectively, is controlled by a dimensionless parameter which accounts for the ratio of the gas pressure inside the device to the liquid viscous pressure drop from the orifices where the liquid is injected to the exit, where the BLS is obtained. This parameter permits the correct scaling of the BLS gas volume fraction of all the experiments presented. © *2004 American Institute of Physics.*
[DOI: 10.1063/1.1737739]

I. INTRODUCTION

Production of bubbles and foams is an area of major importance in chemical and food industry,[1] being the production of small-sized bubbles recognized as a process of major difficulty.[2,3] Readers are referred to Refs. 1–3, and references therein for scientific and industrial applications of bubble and foam generation. One of the well-known and different ways to produce bubbles is to place the needle through which the gas is injected in a coaxial liquid co-flow, which is proved to substantially reduce the bubble diameter with respect to the case in which the surrounding liquid is quiescent.[2,4–6] However, even in this case, the diameter of the bubbles formed scale with the needle injection diameter. As shown in Refs. 3–7, bubbles with sizes much less than the injection needle diameter can be obtained if flow focusing geometry[3,8] is employed. The key idea that permits such size reduction is that the gas is injected within a highly convergent liquid flow that decreases the diameter of the gas ligament (see Fig. 1 in Ref. 3). Through this procedure, and under certain operating conditions, monodisperse bubbles with diameters as small as 10 μm can be produced. However, this method presents two main disadvantages for real industrial applications in which mass production of foams is required. First, the gas fraction $\lambda = Q_g/Q_l$, being Q_g and Q_l the flow rates of gas and liquid, respectively, is limited to very small values [$\sim O(0.1)$ at the outside[3]]. Second, the scale up or multiplexing of these devices is a hard task due to the three-dimensional centering of the injection needles with the exit orifices. A possible alternative to solve the latter problem using the flow focusing concept is to employ a 2D geometry.[9] In this case, the motion of both the focused and focusing fluids develop between two parallel planes. Both the injection needle and the exit orifice can be easily built and centered by using soft lithography methods.[9]

In this paper, we present[10] a new method based on a concept which is between the flow focusing geometry[3,8,9] and the one used in conventional, T-shaped, microchannel devices.[9,11] It will be shown that this new geometrical configuration permits the production of bubble-liquid suspensions (BLS) composed of microbubbles, with large values of λ and it allows the multiplexing in a very easy way. It has to be pointed out that, although the external appearance of the BLS obtained is like that of a foam composed of microbubbles, the term *foam* will not be used to name the resulting product. In effect, most researchers consider a foam to form when the bubbles are polyhedral and, in our case, although the values of λ are relatively high, bubbles arrange in such a way that they keep the sperical shape as will be shown in what follows.

Section II is devoted to the description of the geometry of the device and to the presentation of the experimental

[a)]Electronic mail: gordillo@eurus2.us.es
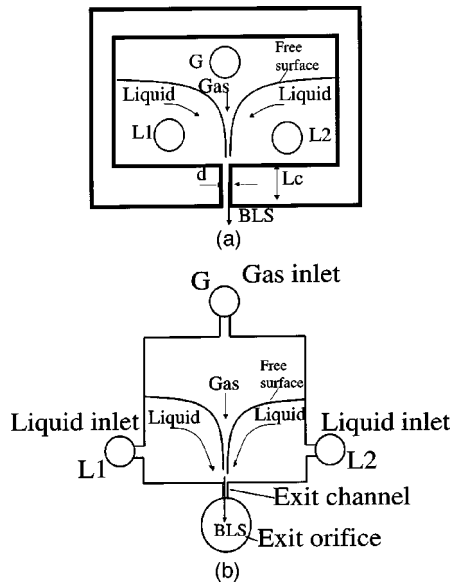[b)]Electronic mail: weitz@deas.harvard.edu

FIG. 1. Front view of a sketch of the device, showing the feeding orifices of both the liquid and the gas, the exit channel and the expected shape of the free surface. In (a), the contour delimited by the thicker line, represents the shape of the thin film used to build the device A; (b) the inlet liquid and gas orifices in device B are connected to the chamber through channels. This is done in order to reduce the chamber deformation.

results. In Sec. III we will deduce, making use of a simple pressure balance, the relevant parameter that controls BLS production. Conclusions are presented in Sec. IV.

II. EXPERIMENTS

In this section we will describe both the geometry of the new microfluidic device and the experimental setup. Measurements of λ for the different geometries and liquids used and for wide ranges of gas pressure and liquid flow rates will also be presented.

A. Description of the device

Consider the front view of the device shown in Fig. 1. In this figure, the circles marked as L_1 and L_2 are holes through which liquid is injected, whereas the circle marked as G is a hole through which gas is supplied into a chamber of small height compared with its lateral dimensions. In fact, the diameters of these orifices in this study, range between 200 μm and 600 μm, whereas both liquid and gas flows discharge in a chamber with a height h (h is normal to the plane of Fig. 1) that varies from 30 μm to 50 μm. The reduced chamber height compared with the size of the orifices, makes the mean combined liquid-gas motion be nearly 2D and develop in a plane which is normal to the direction in which liquid and gas are injected. Basically, the motion develops as in a Hele-Shaw cell. It is important to notice (and essential for the correct operation of this device) that this chamber possesses only one open exit, a channel with a length L_c, width d, and height h. Also, the liquid feeding orifices have to be located at both sides of the exit channel and closer to it than the gas feeding orifice, which is centered between L1 and L2 (see Fig. 1).

TABLE I. σ is the value in mN m^{-1} of air–liquid surface tension, μ is the liquid viscosity in kg m^{-1} s^{-1} and α, β, and γ are the contact angles in degrees with glass, PDMS, and methacrylate, respectively.

Water–glycerine % in volume	Surfactant %	σ	$\mu \times 10^3$	α	β	γ
90/10	0.1	36.9	1.36	45	66	⋯
90/10	0.2	34.3	1.36	⋯	⋯	⋯
80/20	0.1	35.6	1.83	43	55	⋯
70/30	0.1	31.8	2.63	31	55	⋯
60/40	0.2	29.4	3.95	27	53	37
50/50	0.2	28	6.37	25	50	⋯

The devices used to perform the experiments were built using two different techniques. Device A was built by placing a 50 μm thickness kapton sheet between two transparent, parallel, methacrylate plates which were tighten together using screws. The contour delimited by the thicker line in Fig. 1(a) represents the shape of the thin film used to build this device. The feeding holes, that had a diameter of 300 μm, were perforated in one of the plates. The exit channel had a width $d=100\,\mu$m and a length $L_c=500\,\mu$m. The chamber height was $h=50\,\mu$m. The second type of device used, B [see Fig. 1(b)], was built using PDMS soft lithography.[12] The polymer, where the chamber, exit channel and feeding orifices were perforated was stuck to a glass plate. In this case the diameter of the feeding orifices was 600 μm, the chamber height $h\simeq30\,\mu$m and $d=100\,\mu$m and $L_c=500\,\mu$m.

B. Description of the experiments

Liquid was supplied into the chamber through syringe pumps connected to the orifices L1 and L2. The use of these kind of pumps permitted us to control and fix to a given value the liquid flow rate, Q_l. Instead of fixing the incoming gas flow rate, Q_g, we controlled and measured the increment of gas pressure inside the chamber with respect to the atmospheric one, $\Delta\Pi$. Gas pressure was fixed through a valve connected to a pressurized tank, and was measured by using a digital manometer (precision of 0.1%) connected downstream of the valve. The gas pressure drop along the line connecting the valve and the inlet hole G was negligible and, consequently, the manometer provided us with the value of $\Delta\Pi$. The BLS produced discharged directly into the atmosphere and was collected in a calibrated syringe. BLS volume produced in a 3 min experiment permitted us to determine Q_g for a given value of the liquid flow rate. This way of determining the gas flow rate was accurate since we ensured that the bubbles constituting the BLS did not break by using Tween 80, a surfactant mainly used for alimentary purposes. The maximum error in the gas flow rate measurement was estimated to be below 10%. The liquids used were water and glycerine mixtures with a small proportion of Tween 80. The physical properties of the different liquids used are listed in Table I. With regard of the gas, we used both air and nitrogen and no difference in the resulting BLS was observed.

Surface tension was determined using a digital tensiometer and viscosity was measured by means of a rotatory viscosimeter. It has to be pointed out that small changes in
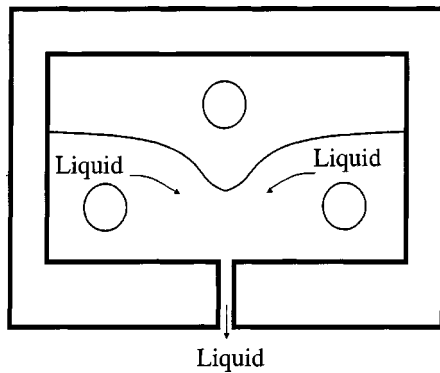
FIG. 2. Sketch of the flow corresponding to regime I.

composition and temperature $[\sim O(10)\,\text{K}]$, produced relative variations in viscosity of a 5% around the value provided in Table I. The contact angle was determined by measuring it directly from the photograph of a small liquid drop placed on a flat, clean surface, of the corresponding material. This method introduced errors in the contact angle measurements of $3°-5°$, which is admissible for our purposes.

When increasing $\Delta\Pi$ from 0 for a given device at a fixed liquid flow rate, we observed three different operating regimes. At low values of $\Delta\Pi$, most of the liquid injected through L1 and L2 exited the chamber through G, leading to the malfunctioning of the device. When the pressure was increased to a value $\Delta\Pi_b$, all the liquid abandoned the chamber through the exit channel steadily and filled it completely. Consequently, no bubbles were generated. This regime (regime I), is sketched in Fig. 2, and is reached for a single value of the gas pressure $\Delta\Pi = \Delta\Pi_b$. A further increase in gas pressure provoked bubbles to be formed within the exit channel, which is now only partially filled with liquid. This regime (regime II), takes place for a pressure range $\Delta\Pi_b < \Delta\Pi < \Delta\Pi_e$. The resulting product is a BLS and thus it constitutes the desired operating condition for which the device was designed. A sketch of this regime together with a picture of the experiment realization is depicted in Fig. 3, showing a steady gas ligament and that bubbles form at the exit channel entrance. Details of the bubble formation process are shown in Fig. 4, where the images were captured using a high shutter speed video camera with a light intensifier. These pictures are a sample of over 100 taken during over 90 min. The fact that consecutive events are found in such a long period of time proves that the bubble formation process is periodic and that gas flow rate does not vary in time for fixed values of Q_l and Q_g. Finally, for gas pressures $\Delta\Pi > \Delta\Pi_e$, the liquid flows attached to the exit channel walls whereas gas flows continuously through the channel core. In this case (regime III), the device operates as a very fine atomizer (see Fig. 5).

Once the different regimes found have been described, we report the gas to liquid volume fraction (λ) of the BLS obtained in regime II as a function of device geometry, liquid properties, $\Delta\Pi$ and Q_l. We proceeded experimentally as follows: first, given a liquid, a device, and for a fixed liquid flow rate, the limiting pressures $\Delta\Pi_{b,e}$ were determined. Next, the value of $\lambda = Q_g/Q_l$ was calculated by measuring
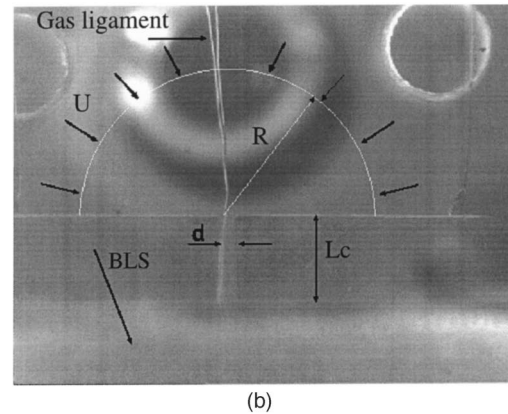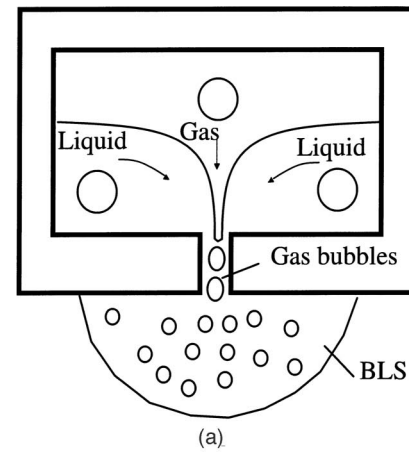

FIG. 3. (a) Sketch of the flow corresponding to regime II. (b) Front view of the device in operating conditions, indicating the dimensions of the exit channel (h is perpendicular to the plane of the figure) and the region where the BLS is generated. The liquid velocity profile which has been assumed along the semicircle is also depicted. Observe that the gas ligament is stable until the exit channel is reached. $Q_l = 10\,\text{ml/h}$ and $\Delta p = 190\,\text{mbar}$. The working fluid is a mixture 60%–40% water–glycerine with a 0.2% of Tween 20.

the BLS volume in the way described previously for three or four values of $\Delta\Pi_b < \Delta\Pi < \Delta\Pi_e$. The results for the devices A and B are shown in Figs. 6 and 7, respectively. As expected, λ increases with increasing $\Delta\Pi$ when Q_l is fixed. The increase in λ is the result of an increase in both the bubble production frequency and volume. However, the bubble diameter is limited by the channel dimensions as observed from Fig. 8, where the bubble sizes of the BLS corresponding to very disparate values of λ are shown.

As demonstrated in Figs. 6 and 7, the BLS characteristics strongly depend on the device geometry, liquid properties, flow rate and gas pressure $\Delta\Pi$. Our purpose in the next section is to predict the gas pressure, as a function of the
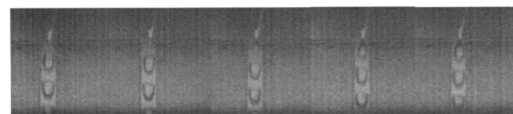

FIG. 4. The figure shows a sequence of five images taken with a high shutter speed camera that illustrates the bubble formation process at the exit channel.
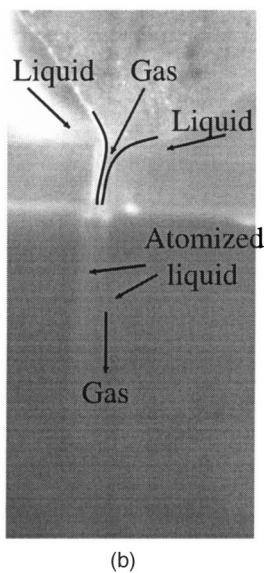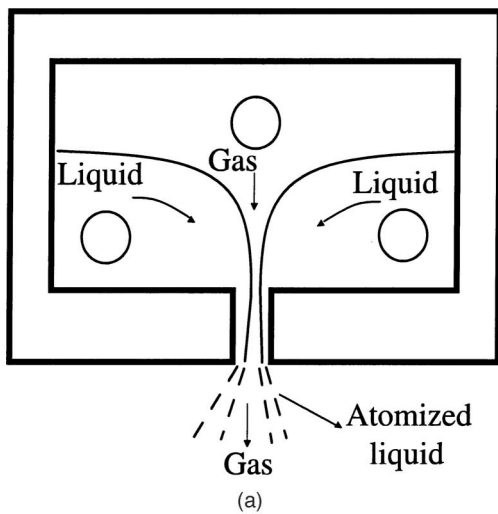
(a)

(b)

FIG. 5. (a) Sketch of the flow corresponding to regime III. (b) Experimental realization of regime III. Notice how the gas flows continuously through the exit channel surrounded by the liquid, which flows attached to the channel walls. A line following the gas–liquid interface inside the chamber has been drawn in order to show that there exists a continuous gap trough which gas exits the pressurized chamber. Outside the device, the atomized liquid is visualized as two separate whiter areas, whereas gas flows between the two atomized zones.
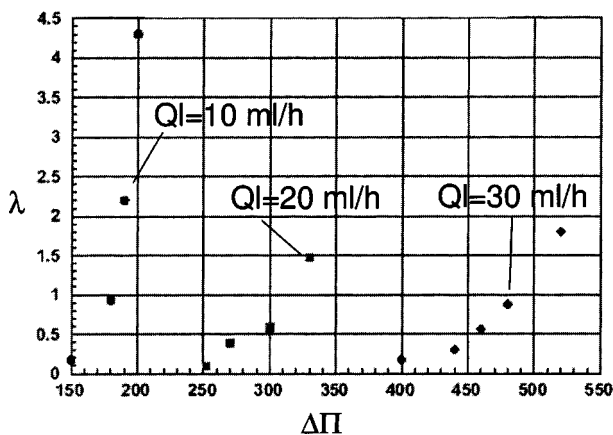

FIG. 6. λ vs $\Delta\Pi$ (in mbars) corresponding to device A. The working fluid is a mixture 60%–40% water–glycerine with a 0.2% of Tween 20.
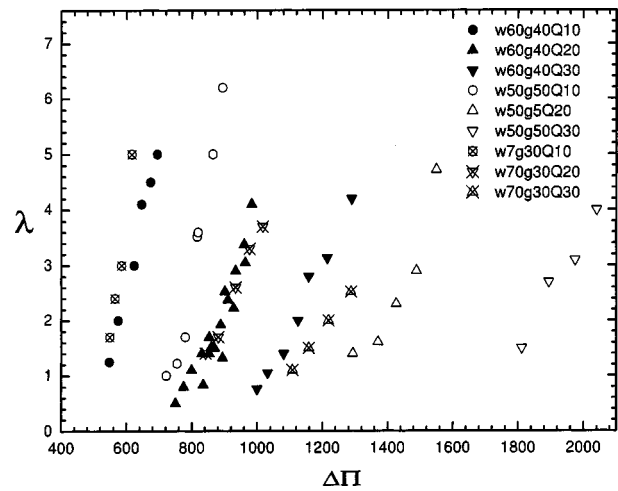

FIG. 7. λ vs $\Delta\Pi$ (in mbars) corresponding to device B. The experimental points are identified in the graph by noticing that W and G and Q represent, respectively, water and glycerine volume fractions in % and that Q means flow rate in ml/h.

different variables, for the regime I to occur, i.e., $\Delta\Pi_b$. Furthermore, based on this pressure, we will define a dimensionless parameter that permits the correct scaling of λ for all the experiments performed.
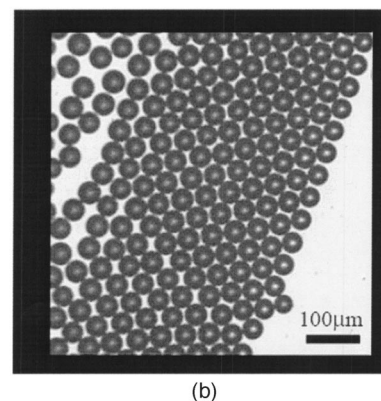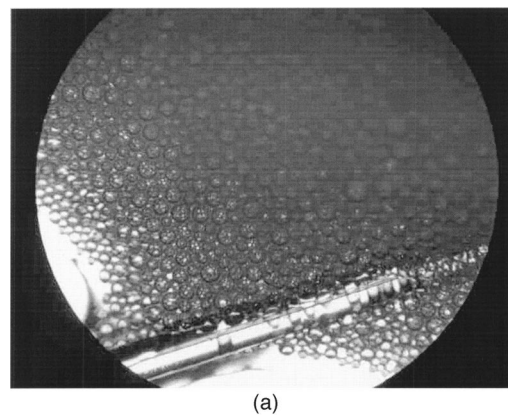

(a)

(b)

FIG. 8. (a) BLS obtained with device A corresponding to the conditions $Q_l = 10$ ml/h and $\Delta p = 200$ mbar ($\lambda = 4.3$). A silica needle of 360 μm of external diameter is inserted in the image in order to estimate the bubble size. The maximum bubble size is ~200 μm. The working fluid is a mixture 60%–40% water–glycerine with a 0.2% of Tween 20. (b) BLS obtained with device B corresponding to the conditions $Q_l = 20$ ml/h and $\Delta p = 1430$ mbar ($\lambda = 2.3$). The maximum bubble size is ~46 μm, and the size reduction with respect to (a) is due to the smaller chamber height. The working fluid is a mixture 50%–50% water–glycerine.

III. MODEL

The calculation of $\Delta\Pi_b$ can be carried out though a simple pressure balance. It is first necessary to determine wether the liquid flow is laminar or turbulent. The liquid Reynolds number inside the chamber can be estimated, in a region near the exit channel, using the typical geometrical dimensions of the devices detailed in Sec. II A and the characteristic physical properties of the liquids in Table I, to give

$$\text{Re}_h = \frac{\rho_l Q_l}{\mu_l d} \sim O(100), \tag{1}$$

where ρ_l and μ_l are the liquid density and viscosity, respectively, and a typical value for Q_l of 20 ml/h has been assumed. The estimation (1) represents the maximum achievable inside the chamber since it is evaluated near the exit channel, where liquid velocities are the largest. Clearly, (1) ensures that the flow is laminar in all cases under study. Furthermore, the liquid velocity profiles will be of Hagen–Poiseuille-type, provided that the distance of the liquid injection orifices to the exit channel be much larger than the entrance length, ℓ_e, which can be estimated as

$$\ell_e \sim 0.1\,\text{Re}_h\,h. \tag{2}$$

This calculation is based on the fact that, for the case of a round pipe of diameter D,[13] $\ell_e \sim 0.05\,\text{Re}_D\,D$. Note that ℓ_e in (2) is an overestimation since, as stated above, Re_h represents the maximum value attainable inside the chamber. Even so, since the typical distance from the exit channel to the liquid inlet orifices is $R \sim 5$ mm,

$$\frac{\ell_e}{R} \sim O(0.1) \ll 1, \tag{3}$$

which proves that velocity profiles are of Hagen–Poiseuille-type both inside the chamber and in the exit channel. Consequently, the liquid pressure drop in regime I inside the channel, Δp_e is given by

$$\Delta p_e = \frac{K_e \mu_l Q_l}{h^4} L_c, \tag{4}$$

where K_e depends on the ratio h/d and can be calculated through a series summation.[14] Moreover, the liquid pressure drop in the chamber, Δp_c, is given by

$$\Delta p_c = \frac{12\mu_l Q_l}{\pi h^3} \ln\frac{2R}{d} = \frac{K_c \mu_l Q_l}{h^3}, \tag{5}$$

where it has been assumed that the liquid in the chamber flows radially from a circle with radius R towards the exit channel [see Fig. 3(b)]. Thus, under the simplifications made, $\Delta\Pi_b$ can be calculated from the next pressure balance

$$\Delta\Pi_b - \frac{2\sigma\cos\theta}{h} \simeq \Delta p_e + \Delta p_c$$

$$= \frac{\mu_l Q_l}{h^3}\left(K_c + K_e\frac{L_c}{h}\right) \rightarrow \alpha_b - \text{Ca}^{-1} = 1, \tag{6}$$
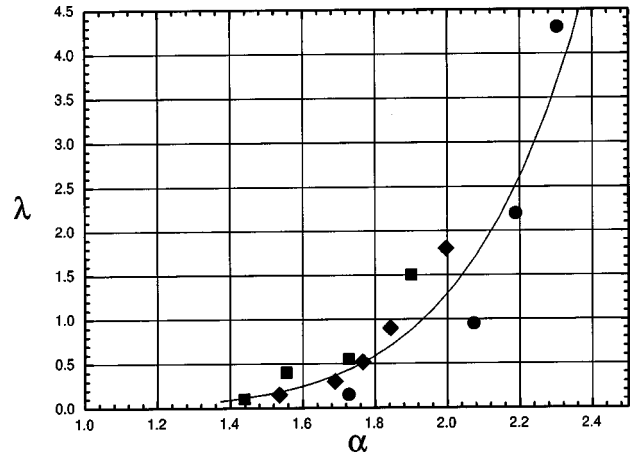
where

FIG. 9. Collapse of the data corresponding to device A (rigid walls) in the α plane. The continuous line represents the best fit to the experimental data. $K_c = 11.44$ [R in (5) is 5 mm] and $K_e = 8.75$.

$$\alpha_b = \frac{\Delta\Pi_b h^3}{\mu_l Q_l}\frac{1}{K_c + K_e L_c/h},$$

$$\text{Ca} = \frac{\mu_l Q_l}{2\sigma\cos\theta h^2}\left(K_c + K_e\frac{L_c}{h}\right), \tag{7}$$

and σ and θ are the gas–liquid surface tension and the contact angle, respectively. Notice that Eq. (6) estates the fact that the liquid pressure at the gas–liquid free surface equals the pressure drop across the chamber and exit channel. In (6), the surface tension pressure jump across the interface has been taken into account in spite that, for the typical values of the different variables in our experiments $\text{Ca}^{-1}/\alpha_b \lesssim O(0.1)$. As an important consequence, bubble formation is not controlled by surface tension as in other related experiments,[15] where the wetting properties of the liquids and materials used affect the stability of the flow patterns obtained. In the subsequent analysis, we will neglect surface tension pressure drop.

Now, we define a parameter α, where

$$\alpha = \frac{\Delta\Pi h^3}{\mu_l Q_l}\frac{1}{K_c + K_e L_c/h}, \tag{8}$$

which is defined analogously to α_b in (7). This parameter permits the correct scaling of the experiments shown in Fig. 6, as depicted in Fig. 9, where the value of λ is represented as a function of the parameter α. Notice that, consistently with the estimation for α_b in (6), $\alpha \sim 1$ for the BLS obtained under the conditions close to regime I, which correspond to values of λ close to zero. But, of most importance is to observe that the collapse of the experimental data is remarkable, in spite of just a single parameter is used to represent the experiments which are subjected to errors of the order of 5%–10% as commented in Sec. II. Clearly, λ should also depend on Re_h and the geometry of the devices used, but this dependence is only slight in view of the result of Fig. 9.

With regard to the results corresponding to the experiments performed with device B, it has to be pointed out that, since the PDMS is elastic, the polymer deforms due to the
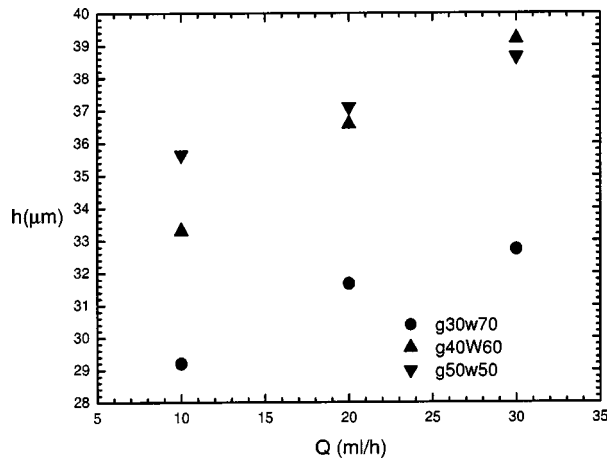
FIG. 10. Different values of the chamber height for device B for each flow rate and liquid viscosity (circles, down triangles, and up triangles corresponding to 70/30, 60/40, and 50/50 water/glycerine mixtures).

FIG. 11. λ vs α for all the experiments performed with devices A and B. The α values corresponding to the experiments performed with device B have been calculated assuming the values of h shown in Fig. 10. The points marked with Mthc are the experimental data obtained with device A. The meaning of w, g, and q, is the same as in Fig. 7. $K_c = 16.23$ [R in (5) is 3.5 mm] and the values of K_e are depicted in Table II.

chamber overpressure $\Delta\Pi$. This introduces a serious complication if a scaling law is intended to be extracted from the experiments since in this case the chamber height depends on the internal pressure, i.e., $h = h(\Delta\Pi)$. This fact introduces a new parameter into the problem which depends on the elasticity of the material used and the geometry of the chamber, making it difficult to obtain universal scaling laws for these kind of devices. Besides, it has to be taken into account that liquid pressure drop is controlled by viscous forces, which depend cubically on h (4)–(5), which enhances the importance of the function $h = h(\Delta\Pi)$. To our knowledge, there are no papers in the literature that overcome this difficulty, which should be present in related studies. In order to present results in a more consistent manner than the one of Fig. 7 we have proceeded assuming, as a starting point, that the experimental law of Fig. 9 is universal. Second, for each pair of values (μ, Q) the height of the device $h(\mu, Q)$, was chosen such that, for the experiments performed with device B, $\alpha \approx 2.1$ at $\lambda = 2$ based on the continuous curve in Fig. 9. Figure 10 shows the chamber height obtained through this procedure as a function of the flow rate and kind of liquid used. Notice that the chamber height is always very close to the nominal height, $h = 30 \, \mu$m, and that it increases with the flow rate and liquid viscosity, consistently with the larger pressures existing inside the chamber.

Figure 11 shows the experimental results of Figs. 6 and 7 in the α–λ plane, where the values of α corresponding to the experiments performed with device B have been calculated using the chamber height depicted in Fig. 10 and the values of K_e provided in Table II. The result in Fig. 11 is not a rigorous proof of the universality of the law obtained in Fig. 9, but the fact that the good collapse shown in Fig. 11 has been obtained with consistent values of the chamber height for the experiments performed with device B, points out to the importance of α (which is always of order unity) as an essential parameter to describe bubble production using the geometry proposed in this paper. Anyway, the procedure used to scale the experiments performed with device B, is efficient in the sense that it permits to express the value of λ
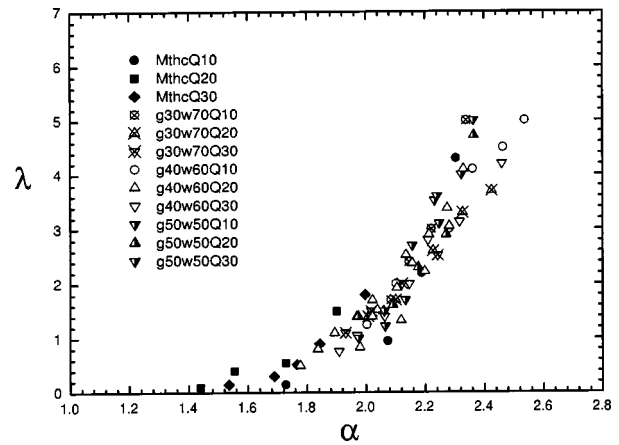
under different conditions providing the value of α and the value of h as a function of the liquid flow rate and liquid viscosity.

Finally, it has to be pointed out that we have only provided a simple characterization of the flow (λ as a function of the parameters of the problem through the dimensionless parameter α). With regard to bubble size, its scaling with the different parameters of the flow needs further research. However, it can be anticipated that, in view of the experiments shown in Figs. 4–8, bubble size is determined by two different mechanisms: the primary formation mechanism (shown in Fig. 4), and the possible bubble coalescence that take place outside the exit channel. In any case, it can be deduced from Figs. 4–8, that maximum bubble diameter scales with the exit channel dimensions. This fact implies that the reduced dimensions of the exit channels employed in these devices, ensures that the BLS obtained will be composed of bubbles whose diameters, d_b, are of the order of $d_b \sim O(10-100) \, \mu$m.

IV. CONCLUSIONS

In this paper we have presented a new kind of microfluidic device that is between the 2D flow focusing geometry used in Ref. 9 and that employed in conventional, T-shaped microchannels.[11] Using this procedure it has been shown that BLS with large values of gas fraction λ and composed of micron-sized bubbles can be obtained. Using a simple pressure balance we have deduced the order unity dimensionless

TABLE II. Values of the constants K_e for device B calculated using the chamber heights shown in Fig. 10.

Q_l (ml/h)	G30W70	G40W60	G50W50
10	4.26	5.1	5.49
20	4.73	5.69	5.79
30	4.92	6.2	6.12

parameter, α, which correctly scales the experimentally obtained gas to liquid BLS volume fraction performed with device A as a function of the different variables of the problem: device geometry, liquid properties, liquid flow rate and gas pressure. In the case of device B, where an elastic polymer (PDMS) is used to build the chamber, the difficulty of determining $h(\Delta\Pi)$ has been overcome by assuming that the experimental law obtained with device A is universal. Although not rigorously, this starting hypothesis is supported in view of the collapse shown in Fig. 11, which is obtained with values of the chamber height that are consistent with the liquid properties and the liquid flow rates. In any case, the procedure followed to scale the experiments performed with device B, is efficient since it permits to express the value of λ under different conditions only providing the value of α and the value of h as a function of the pair of values (μ, Q). Also, as shown in Fig. 5, these kinds of devices can be used as very fine atomizers for $\Delta\Pi > \Delta\Pi_e$, with scaling laws for the drops obtained that should be similar to those of Ref. 8. Finally, the multiplexing of this kind of devices is straightforward, since a horizontal array of the device shown in Fig. 1 would permit mass BLS (and foam) production and its use in industrial applications.

ACKNOWLEDGMENTS

[1] H. A. Stone, S. A. Koehler, S. Hilgenfeldt, and M. Durand, "Perspectives on foam drainage and the influence of interfacial rheology," J. Phys.: Condens. Matter **15**, S283 (2003).

[2] H. N. Oguz and A. Prosperetti, "Dynamics of bubble growth and detachment from a needle," J. Fluid Mech. **257**, 111 (1993).

[3] A. M. Gañán-Calvo and J. M. Gordillo, "Perfectly monodisperse microbubbling by capillary flow focusing," Phys. Rev. Lett. **87**, 274501 (2001).

[4] S. C. Chuang and V. W. Goldschmidt, "Bubble formation due to a submerged capillary tube in quiescent and coflowing streams," Trans. ASME D: J. Basic Eng. **92**, 705 (1970).

[5] R. A. M. Al-Hayes and R. H. S. Winterton, "Bubble diameter on detachment in flowing liquids," Int. J. Heat Mass Transfer **24**, 223 (1981).

[6] H. Tsuge, S. I. Hibino, and Y. Nojima, "Volume of a bubble formed at a single submerged orifice in flowing liquid," Int. Chem. Eng. **21**, 630 (1981).

[7] J. M. Gordillo, A. M. Gañán-Calvo, and M. Pérez-Saborid, "Monodisperse microbubbling: Absolute instabilities in coflowing gas–liquid jets," Phys. Fluids **13**, 3839 (2001).

[8] A. M. Gañán-Calvo, "Generation of steady liquid microthreads and micron-sized monodisperse sprays in gas streams," Phys. Rev. Lett. **80**, 285 (1998).

[9] S. L. Anna, N. Bontoux, and H. A. Stone, "Formation of dispersions using flow focusing in microchannels," Appl. Phys. Lett. **82**, 364 (2003).

[10] J. M. Gordillo and A. M. Gañán-Calvo, Spanish Patent No. P200300169 (2003).

[11] J. B. Knight, A. Vishwanath, J. P. Brody, and R. H. Austin, "Hydrodynamic focusing on a silicon chip: Mixing nanoliters in microseconds," Phys. Rev. Lett. **80**, 3863 (1998).

[12] J. C. McDonald, D. C. Duffy, J. R. Anderson, D. T. Chiu, H. Wu, O. J. A. Schueller, and G. M. Whitesides, "Fabrication of microfluidic systems in poly(dimethylsiloxane)," Electrophoresis **21**, 27 (2000).

[13] *Laminar Boundary Layers*, edited by L. Rosenhead (Dover, New York, 1988).

[14] C. A. J. Fletcher, *Computational Techniques for Fluid Dynamics*, Springer Series in Computational Physics (Springer, Berlin, 1991), Vol. 1.

[15] R. Dreyfus, P. Tabeling, and H. Willaime, "Ordered and disordered patterns in two-phase flows in microchannels," Phys. Rev. Lett. **90**, 144505 (2003).